sustainability

MDPI

Article

Dynamic Shear Strength Characteristics of Lightweight Sand-EPS Soil

Liping Zhu [1,2], Kejun Wen [3], Ruiming Tong [2] and Mingdong Li [4,*]

[1] School of Water Resources and Environmental Engineering, East China University of Technology, Nanchang 330013, China; zlp1123@ecut.edu.cn
[2] Key Laboratory of Ministry of Education for Geomechanics and Embankment Engineering, Hohai University, Nanjing 210098, China; m20l@163.com
[3] Department of Civil and Environmental Engineering, Jackson State University, Jackson, MS 39217, USA; kejun.wen@jsums.edu
[4] School of Civil and Architectural Engineering, East China University of Technology, Nanchang 330013, China
* Correspondence: ytlimd@163.com

Abstract: Lightweight sand–EPS soil (LSES) is regarded as a kind of sustainable geomaterial for providing a way to reutilize fast-growing waste expanded polystyrene (EPS) packages. It is usually applied in marine geotechnical engineering to solve the excessive settling of soft ground or bumps at bridge heads due to its merits such as low density, high strength, and adjustability. Aiming to investigate the dynamic shear strength of LSES made from marine sand, a series of laboratory dynamic triaxial experiments was conducted on LSES with different proportions and control sand (CS). The influences of cement content, EPS bead content, and confining pressure on dynamic shear strength were analyzed, as were comparisons with the material sand. It was found that the dynamic strength of LSES increased with the increase in cement content and confining pressure. The bonding function of cement hydration products contributed to the dynamic strength of LSES; however, the work required a certain content of cement. The dynamic strength of LSES decreased with the increase in EPS bead content due to the low particle strength and smooth surface of EPS beads. The cyclic number of failure (N_f) of both LSES and CS decreased linearly with the increase in dynamic shear stress in semilogarithmic coordinates. Both the slopes and the intercepts increased with the increase in cement content and confining pressure. However, they decreased with the increase in EPS bead content.

Keywords: lightweight soil; dynamic strength; sand; EPS beads; cohesion; friction angle

Citation: Zhu, L.; Wen, K.; Tong, R.; Li, M. Dynamic Shear Strength Characteristics of Lightweight Sand-EPS Soil. *Sustainability* **2022**, *14*, 7397. https://doi.org/10.3390/su14127397

Academic Editors: Chao Jia, Kai Yao and Shuai Shao

Received: 5 May 2022
Accepted: 14 June 2022
Published: 16 June 2022

1. Introduction

In the marine area, deep soft sediments have always been a significant engineering geology challenge, resulting in continuous excessive settling of public infrastructures, especially undue settling causing the cracking of pavement and bumps at bridge heads [1]. Meanwhile, from clothing packaging to food packaging, expanded polystyrene (EPS) is being used on an increasing scale, especially after COVID-19, which further dramatically increased the use of disposable EPS [2]. The reutilization of waste EPS packing boxes to produce lightweight sand–EPS soil (LSES) is a good way to protect the environment and to solve the engineering geology challenge of marine deep soft sediments [3].

LSES is a kind of geotechnical material with many merits, such as lightness [4], adjustability of strength/density [5], and fluidity [6]. It has been widely applied in many engineering applications, including slope fill [7,8], soft foundation treatment [9], backfill of pipelines [10–13], highway broadening [1], etc., as shown in Figure 1, and are known as "green construction". The static engineering properties of LSES have been investigated a lot. Its dry density is controlled by the EPS bead content. Its shear strength linearly increases with cement content and hyperbolically decreases with EPS bead content. Its

cohesion increases with cement content because it is contributed by cement hydration products. Its friction angle decreases with EPS bead content due to their smooth surface. Furthermore, quantitative relationships have been provided [4,5,14–17]. As for the application in transportation infrastructure, as well as the response under earthquakes, the dynamic properties must be referred to. For cyclic axial strain greater than 1.0%, LSES exhibits a visco–elasto–plastic behavior associated with the occurrence of permanent plastic strains. The backbone curve of LSES is nonlinear, with a strain-hardening characteristic [18], include a vibration compaction stage, vibration shear stage, and vibration failure stage [1]. In addition, the backbone curves of SLES tends to increase with the increase in cement content and confining pressure, which indicates that increase in cement content and confining pressure could improve its dynamic strength and dynamic stiffness [19]. A modified Hardin–Drnevich model was established by [18] to effectively predict results of the backbone curves of LSES. Moreover, the simulation study on the process of falling rock found that LSES could reduce the impact of falling rocks [20].

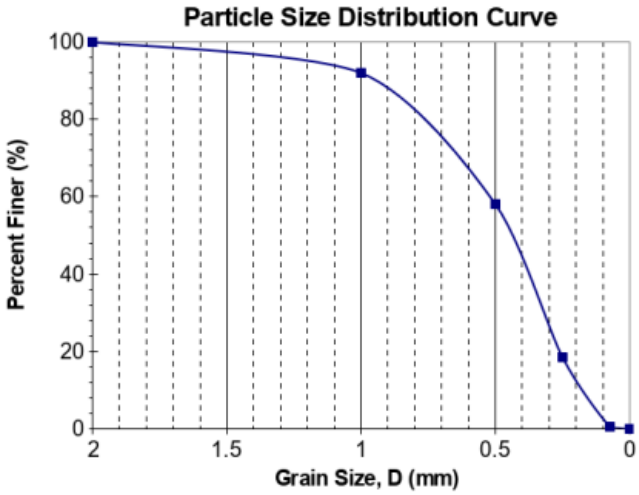

Figure 1. Particle size distribution of material marine sand.

Aiming to investigate the dynamic strength characteristics of LSES made of marine sand, which represents its bearing capacity under reciprocating cyclic load/seismic action [21], a series of laboratory cyclic triaxial tests on LSES with different proportions was carried out. The dynamic strength characteristics of LSES were observed. The influences of cement content, EPS bead content, and confining pressure on the dynamic strength of LSES were analyzed. The results were also compared with those of control sand (CS). The work is novel, and the results will introduce the applications of LSES in coastland.

2. Materials and Methods

2.1. Materials

The LSES was made from marine sand, EPS beads, cement, and water. Marine sand also worked as control samples. The material sand used in this study was taken from the estuary of the Yangtze River, Chongming, Shanghai, China. Its specific gravity was 2.71 and its particle size distribution is shown in Figure 1, which indicates that the particles were mainly in the scope of 0.1–1 mm. It was classified as poorly graded sand according to the Unified Soil Classification System [22]. As for chemical composition, more than 97% of the sand was silica.

The binder used in the experiment was #32.5 Portland cement produced by Zhongshan cement factory in Nanjing, China, with a water–cement ratio of 1.2. The properties of the cement are listed in Table 1.

Table 1. Fundamental properties of the cement.

Item	Value
Density	1.3 g/cm^3
Specific density	3.0 g/cm^3
Fineness (residue on 0.08 mm sieve)	2.50%
Normal consistency	25.2%
Initial setting time	2:35
Final setting time	3:50
3d fracture resistance	3.8 MPa
28d fracture resistance	8.0 MPa
3d compression strength	16.0 MPa
28d compression strength	42.0 MPa

The EPS beads are a macromolecule polymer with prior lightweight properties. The EPS beads used in this study are produced by Youbang Plastics Co. LTD, Nanjing, China, as shown in Figure 2. They were 0.0132 g/cm^3 in bulk density and 2 mm in average diameter.

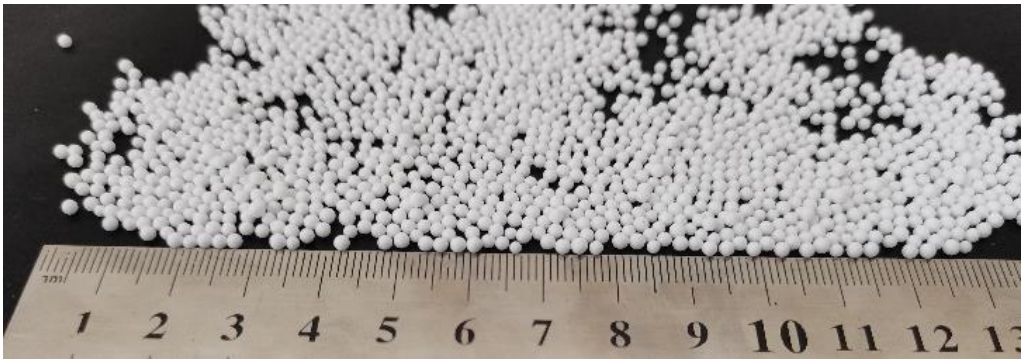

Figure 2. Photograph of EPS beads.

2.2. Material Proportions of LSES

Aiming to investigate the influences of cement content and EPS bead content on the dynamic shear strength characteristics, a total of 8 LSESs were tested in this study. Their detailed material proportions are listed in Table 2, in which C_{eps} indicates the volumetric content of EPS beads, C_c indicates the cement content by weight of dry soil, m_{eps} indicates the mass of the EPS beads, m_s indicates the mass of the sand, and m_c indicates the mass of the cement.

Table 2. The volume content of EPS beads and the proportion of cement.

Marker	Material Proportions		Mass of Materials		
	C_c (%)	C_{eps} (%)	m_{eps} (g)	m_s (g)	m_c (g)
Sand	0	0	0	700.0	0
3–10	3	10	1.134	630.0	18.9
3–20	3	20	2.268	560.0	16.8
3–30	3	30	3.402	490.1	14.7
3–40	3	40	4.536	420.1	12.6
6–40	6	40	4.536	420.1	25.2
9–40	9	40	4.536	420.1	37.8
12–40	12	40	4.536	420.1	50.4

2.3. Preparation of Specimens

The preparation of specimens is shown in Figure 3. All materials were measured and put into a blender. They were stirred to be uniform at a speed of 50 rot/min for 5 min. The

mixtures were then put into a mold, which was 61.8 mm in diameter and 140 mm in height. The target void ratio was 0.62. Each specimen was compacted in 5 layers [5]. Four samples were prepared for each dosage of LSES. The specimens were cured in an oven at 20 °C and 99% humidity for 28 days. After being cured, the specimens were put into an air extractor and vacuumized for 20 min at a vacuum degree of −0.1 MPa. Finally, the specimens were fully saturated by opening the water inlet valve, and then soaked in water for 24 h.

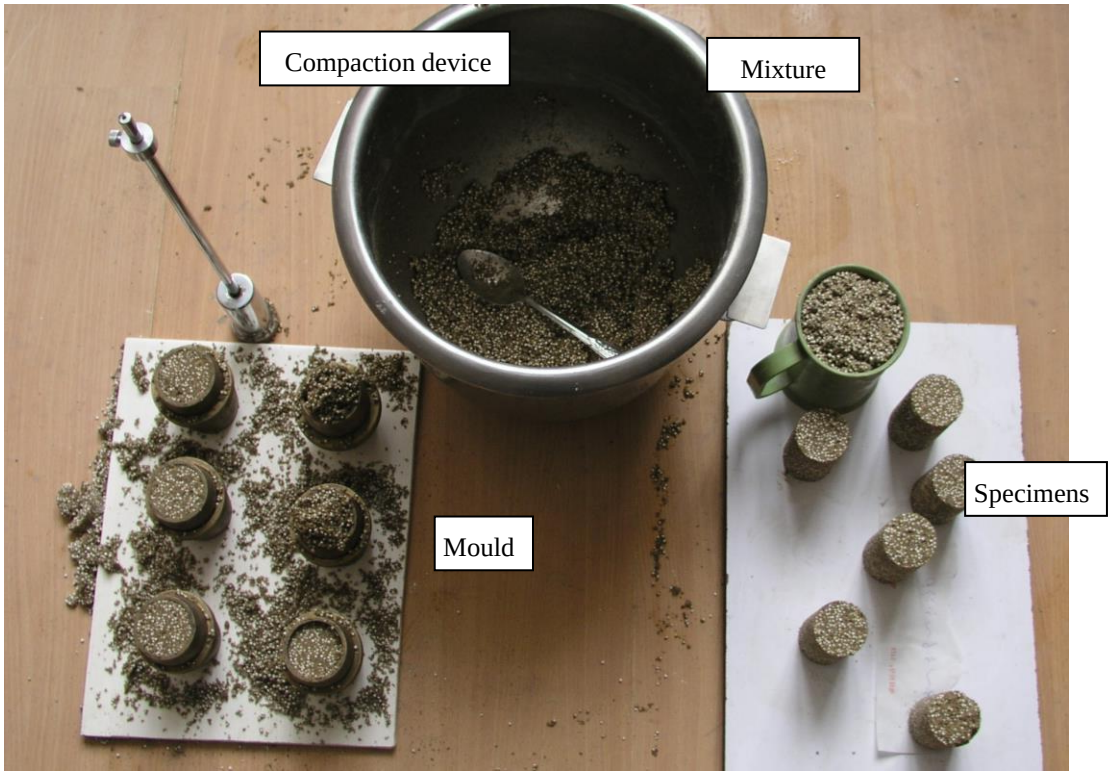

Figure 3. Preparation of specimens.

2.4. Test Methods

The specimens were tested by a multi-functional automatic dynamic triaxial apparatus developed by Hohai University, Nanjing, China and Round Well Co., Ltd, Tokoy, Japan. The samples were placed in the cell that connected the vibration equipment. A cell pressure of 20 kPa was applied to saturate the pipeline until no air bubbles remained in the drainage pipe. A vacuum pressure of 100 kPa was then applied to saturate the samples. Certain confining pressures (60, 90, and 120 kPa) were applied to consolidate each sample. The consolidation processes were carried out until the volume change of the sample in 5 min was less than 0.1 mL. After that, undrained dynamic shear tests were conducted under sine dynamic load with a frequency of 0.1 Hz. The amplitude of dynamic shear stress was controlled by the dynamic shear stress ratio, as shown in Equation (1), which was 0.5, 0.6, 0.7, and 0.8, respectively.

$$s = \frac{\tau_d}{\sigma_c} = \frac{\sigma_d}{2\sigma_c} \quad (1)$$

where

s is the dynamic shear stress ratio;
τ_d is the maximum dynamic shear stress;
σ_c is confining pressure for consolidation;
σ_d is deviatoric stress.

3. Results and Discussion

3.1. Identification and Presentaion of the Dynamic Shear Strength of LSES

Figure 4 shows a typical dynamic deformation curve of LSES. The specimen was 6–40, the confining pressure was 90 kPa, and s was 0.8. At the beginning, the maximum dynamic strain of LSES developed with the increase in loading cycles gradually, which can be called the deformation developing stage. After that, the maximum dynamic strain of LSES kept at a level with the increase in the number of cycles, which can be called the deformation maintaining stage. Last, the maximum dynamic strain of LSES started to decline. As is known, there are four common criteria for dynamic shear failure, including the pore water pressure criterion, ultimate equilibrium criterion, maximum strain criterion, and yield failure criterion [21]. Since the EPS beads contained bubbles, the pore water pressure criterion and the ultimate equilibrium criterion were not applicable for LSES. The failure strain of LSES was generally less than 2%, which is much less than the maximum strain criterion of 5% or 10%; thus, the maximum strain criterion was not applicable for LSES. Based on the yield failure criterion, the decline in maximum dynamic strain of LSES can be regarded as the failure of LSES. Therefore, the last stage can be called the failure stage. Taking this typical dynamic deformation curve, for example, the failure number of loading cycles (N_f) was 30 [18]. That is to say, an LSES of 6–40 will fail after 30 loading cycles when the dynamic shear stress ($\sigma_d/2$) is 72 kPa, which is obtained by Equation (2).

$$\tau_d = s\sigma_c = 0.8 \times 90 = 72 \text{ kPa} \quad (2)$$

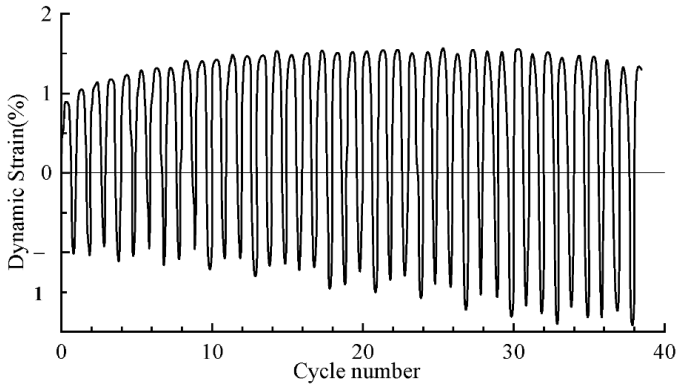

Figure 4. A typical dynamic deformation curve of LSES (specimen was 6–40, confining pressure = 90 kPa, s = 0.8).

3.2. Effect of EPS Bead Content on Dynamic Shear Strength

The relationships between the dynamic shear strength ($\sigma_d/2$) and failure number of loading cycles (N_f) of the LSES and sand are shown in Figure 5. It is clear that the N_f of both the LSES and sand decreased with the increase in dynamic shear stress. For the relationships to fit the linear relationship well, they can be expressed with Equations (3) and (4). Moreover, the dynamic shear strength of the LSES decreased with the increase in EPS bead content. When the EPS bead content was 10%, 20%, or 30%, the relationship curve between the dynamic shear strength and N_f was higher than that of sand. When the EPS bead content was 40%, the relationship curve between the dynamic shear strength and N_f was lower than that of sand. The possible reason is that the soil skeleton was too small in the specimen cross-section when the EPS bead content was exorbitant, and then little dynamic shear stress occurred when the effective stress increased. It was revealed that the increasing EPS bead content obviously reduced the dynamic strength of EPS composite soil, which is the same as the results in this study [23]. It was reported that the shear strength of clay/EPS particulate mixtures was relatively unaffected by the EPS content [24], which is different from the results in this study. The reason is probably due to the different grade of EPS.

$$\sigma_d/2 = a - b \lg N_f \quad (3)$$

$$b = -[\Delta(\sigma_d/2)/\Delta \lg N_f] \text{ (kPa)} \quad (4)$$

where

$\sigma_d/2$ is the dynamic shear strength (kPa);
N_f is the failure number of loading cycles;
a is the intercept of the line, which represents the dynamic shear strength when N_f is 1;
b is curve's slope, which represents the decrease in dynamic shear strength with N_f in logarithmic.

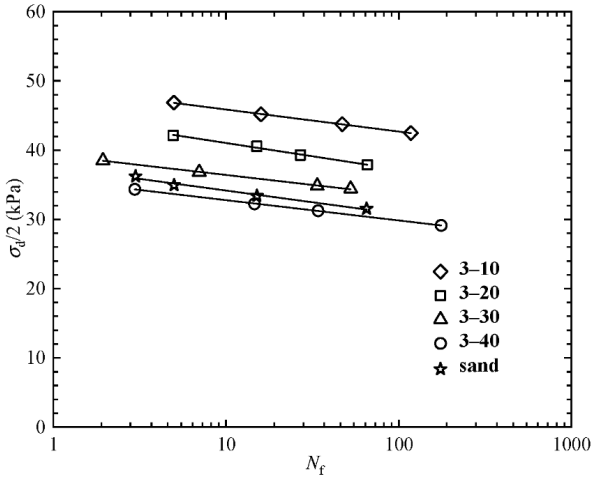

Figure 5. The ($\sigma_d/2$~N_f) curve of sand and LSES of different EPS bead contents.

3.3. Effect of Cement Content on Dynamic Shear Strength of LSES

The $\sigma_d/2$~N_f curves of the LSES with 40% EPS bead content and sand are shown in Figure 6. It can be found that the dynamic shear strength of LSES increased with the increase in cement content. Ref. [23] reported that the increasing cement content effectively improved the dynamic strength of EPS composite soil, which is in agreement with this result. When cement content was 3%, the relationship between the dynamic shear strength and N_f of LSES was similar to that of sand. When the cement content was 6%, 9%, or 12%, the decrease in dynamic shear strength of LSES with N_f in logarithmic was larger than that of sand, indicating that the dynamic shear strength decreased more sharply than the sand. This may have resulted from the increase in brittleness of the LSES due to the addition of cement, which weakened the ability to resist cyclic loading.

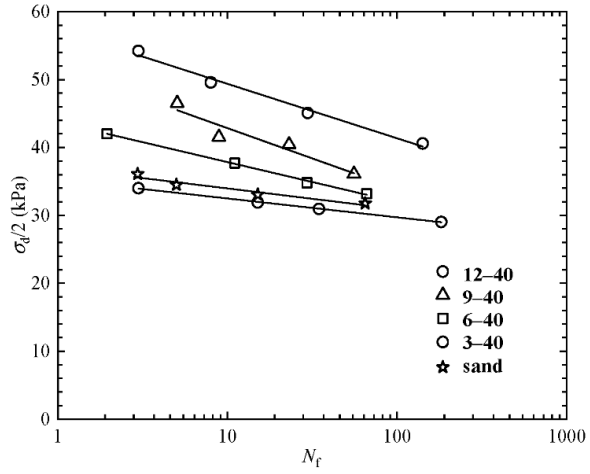

Figure 6. The $\sigma_d/2$~N_f curve of LSES of different cement contents and sand.

3.4. Effect of Confining Pressure on Dynamic Shear Strength of LSES

The $\sigma_d/2$~N_f curve of the LSES of 9–40 and sand at different confining pressures are shown in Figure 7. The dynamic strength of the LSES and pure sand increased with the increase in confining pressure. It can be seen that the change law of dynamic strength and static strength of the LSES with confining pressure was the same. In the same confining pressure, the dynamic shear strength of the LSES of 9–40 was higher than that of pure sand. This indicates that the dynamic load required to break the LSES was significantly greater than that required for pure sand. However, the differences decreased with the increase in N_f. This could be due to the special strength mechanism and failure process of LSES. LSES is formed by wrapping sand particles and EPS beads with cement hydrate. Therefore, the strength of the LSES samples mainly depended on the strength of the cement hydration products. At the initial stage of dynamic load, the LSES samples were intact, and the sand particles and EPS beads were effectively covered by cement hydration products. Therefore, the dynamic load required to damage the LSES in fewer loading cycles was large. When LSES is subjected to dynamic loading continually, the cement hydration products suffer from concentrated stress. When the concentrated stress reaches the strength of the cement hydrate, microcracks occur, and then the cracks expand and connect with each other. After that, the sand particles and EPS beads disperse and separate from each other to fill the cracks. Therefore, the positive strain decrease forms the typical failure performance of LSES. All these results are in complete agreement with the results of other soils [18,25,26].

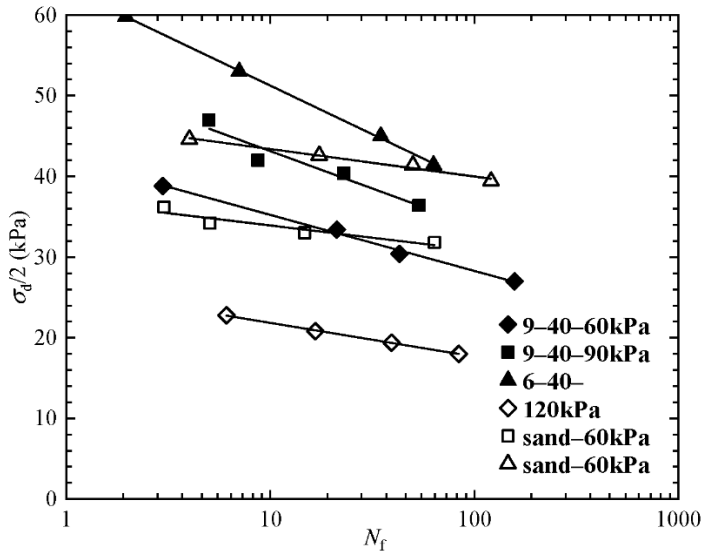

Figure 7. $\sigma_d/2$~N_f curve of sand and LSES sample with different confining pressure.

3.5. Dynamic Mohr Circle and Dynamic Strength Parameters of LSES

The dynamic Mohr circle and failure envelope of the LSES of 9–40 and sand at confining pressures of 60, 90, and 120 kPa are shown in Figures 8 and 9, respectively. The dynamic Mohr stress circle was divided into a compression stress semi-circle and tensile stress semi-circle. The consolidation stress was considered the starting point of the stress circle, and the dynamic stress was taken as the radius to draw a semicircle in both the positive and negative directions of the horizontal axis. For example, point A indicates the consolidation stress in Figure 7, and semi-circles 1 and 2 are tensile and compression stress, respectively. It can be seen that the tensile stress semi-circle failed first, and the failure envelope of the stress circle was drawn based on the tensile stress semi-circle. The intercept of the failure envelope indicates cohesion (c_d) and the incline angle indicates friction angle (φ_d). The dynamic cohesion c_d of the LSES of 9–40 and sand were 28.5 kPa and 0 kPa, respectively. The cohesion of the LSES was enhanced due to the binding of the cement hydrate. The dynamic friction angle φ_d of the LSES of 9–40 and sand were 21.8° and 31.4°,

respectively. This means that dynamic friction angle of the LSES was smaller than that of sand. This could be due to the smooth surface of the EPS beads. This is in agreement with what [22] reported, in that the addition of EPS beads led to an increase in the cohesion, as well as to a reduction in the friction angle.

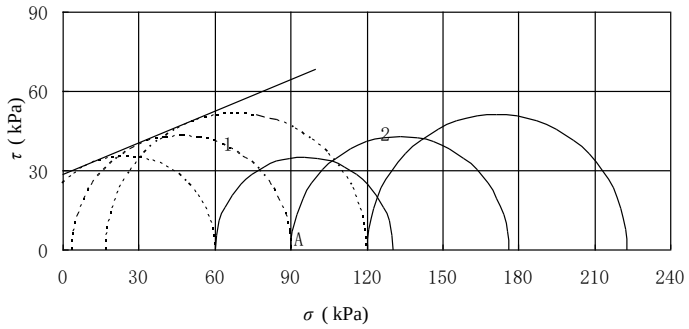

Figure 8. Dynamic Mohr circle and failure envelope of LSES of 9–40 under different confining pressures.

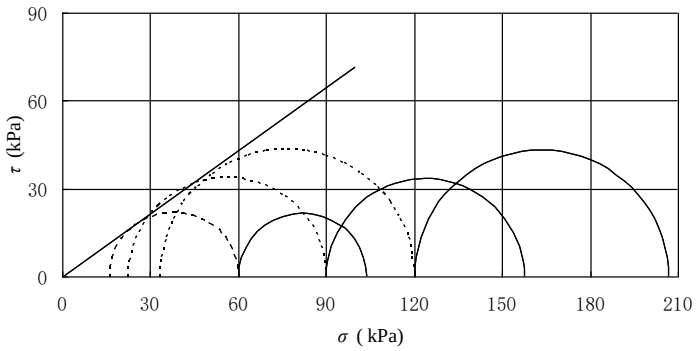

Figure 9. Dynamic Mohr circle and failure envelope of sands under different confining pressures.

4. Conclusions

Based on the indoor dynamic shear strength tests of LSES and material sand, the dynamic strength of LSES increased with the increase in cement content and confining pressure. The bonding function of cement hydration products contributed the dynamic strength of LSES; however, the work required a certain content of cement. The dynamic strength of LSES decreased with the increase in EPS bead content due to the low particle strength and smooth surface of the EPS beads. The logarithms of the Nfs of both LSES and the material sand decreased with the increase in τ_d in linear. Both the slopes and the intercepts of the τ_d~lnN_f curves increased with the increase in cement content and confining pressure. The intercept of the τ_d~lnN_f curves decreased with EPS bead content.

Author Contributions: Conceptualization, M.L.; Writing—original draft, L.Z.; Writing—review & editing, K.W. and R.T. All authors have read and agreed to the published version of the manuscript.

Funding: This research was funded by National Foundation of China under grant No. 51869001, the Key Laboratory of Ministry of Education for Geomechanics and Embankment Engineering (B210204004), the Key Research and Development Program of Jiangxi Province under grant No. 20202BBG73037, and the Foundation of Engineering Research Center for Geological Environment and Underground Space of Jiangxi Province (JXDHJJ2021-013).

Institutional Review Board Statement: Not applicable.

Informed Consent Statement: Not applicable.

Data Availability Statement: The data presented in this study are available on request from the corresponding author via email ytlimd@163.com.

Acknowledgments: The Funders are gratefully acknowledged.

Conflicts of Interest: The authors declare no conflict of interest.

References

1. Zhou, Y.; Li, M.; Wen, K.; Tong, R. Stress-strain behaviour of reinforced dredged sediment and expanded polystyrenes mixture under cyclic loading. *Geomech. Eng.* **2019**, *6*, 507–513.
2. Vaverková, M.D.; Paleologos, E.K.; Dominijanni, A.; Koda, E.; Tang, C.; Małgorzata, W.; Li, Q.; Guarena, N.; Mohamed, A.O.; Vieira, C.S.; et al. Municipal solid waste management under COVID-19: Challenges and recommendations. *Environ. Geotech.* **2021**, *8*, 217–232. [CrossRef]
3. Kaewunruen, S.; Qin, Z.J. Sustainability of Vibration Mitigation Methods Using Meta-Materials/Structures along Railway Corridors Exposed to Adverse Weather Conditions. *Sustainability* **2020**, *12*, 24. [CrossRef]
4. Zou, W.; Wan, L.; Han, Z.; Wang, X. Effect of stress history on compressive and rheological behaviors of EPS geofoam. *Constr. Build. Mater.* **2019**, *228*, 201907318. [CrossRef]
5. Li, M.; Wen, K.; Li, L.; Tian, A. Mechanical properties of expanded polystyrene beads stabilized lightweight soil. *Geomech. Eng.* **2017**, *13*, 459–474.
6. Liu, H. Technological innovation methods and practices in geotechnical engineering. *Chin. J. Geotech. Eng.* **2013**, *35*, 34–58.
7. Duan, X.; Hou, T.; Jiang, X. Study on stability of exit slope of Chenjiapo tunnel under extreme rainstorm conditions. *Nat. Hazards* **2021**, *107*, 1387–1411. [CrossRef]
8. Zhang, J.; Li, M.; Ke, L.; Yi, J. Distributions of lateral earth pressure behind rock-socketed circular diaphragm walls considering radial deflection. *Comput. Geotech.* **2022**, *143*, 104604. [CrossRef]
9. Yang, X.; Chandra, D.; Hanlong, L. Testing and Modeling on Particle Breakage for Granular Soils. *Int. J. Geomech.* **2021**, *21*, 0002186.
10. Abdollahi, M.; Tafreshi, S.N.M.; Leshchinsky, B. Experimental-numerical assessment of geogrid-EPS systems for protecting buried utilities. *Geosynth. Int.* **2019**, *26*, 333–353. [CrossRef]
11. Abdollahi, M.; Tafreshi, S.N.M.; Leshchinsky, B. Protection of Buried Utilities against Repeated Loading: Application of Geogrid-EPS Geofoam System. *Int. J. Geomech.* **2021**, *21*, 04021158. [CrossRef]
12. Arvin, M.R.; Ghafary, G.R.; Hataf, N.; Ghafary, A.R. Shear behavior of EPS geofoam reinforced with polypropylene fiber. *Geomech. Eng.* **2021**, *25*, 347–355.
13. Yang, Z.; Zhang, Q.; Yang, Z.; Shi, W.; Lv, J.; Lu, Z.; Ling, X. Advances in properties of rubber reinforced soil. *Adv. Civ. Eng.* **2020**, *2020*, 6629757. [CrossRef]
14. Cai, X.; Gao, H.; Zhao, H.; Chen, G.; Chen, R. Dynamic characteristics of EPS beads composite lightweight soil under railway loading. *J. Disaster Prev. Mitig. Eng.* **2015**, *35*, 651–658.
15. Gao, H.; Chen, R.; Tong, F.; Chen, G.; Cai, X. Dynamic modulus and damping ratio of EPS bead composite soil under complex stress conditions. *J. Disaster Prev. Mitig. Eng.* **2015**, *35*, 166–172; discussion 198.
16. Tasalloti, A.; Chiaro, G.; Murali, A.; Banasiak, L. Physical and mechanical properties of granulated rubber mixed with granular soils-a literature review. *Sustainability* **2021**, *13*, 4309. [CrossRef]
17. Yang, X.; Yifan, T.; Guoliang, M.; John, S.M.; Jian, C. Thermal Conductivity of Biocemented Graded Sands. *J. Geotech. Geoenvironm. Eng.* **2021**, *147*, 04021106.
18. Hou, T.; Pei, Z.; Luo, Y.; Cui, Y. Dynamic deformation characteristics and modified Hardin-Drnevich model for light weight soil mixed with EPS particles. *Chin. J. Geotech. Eng.* **2021**, *43*, 1602–1611.
19. Zhou, Y.; Li, M.; He, Q.; Wen, K. Deformation and damping characteristics of lightweight clay-EPS soil under cyclic loading. *Adv. Civ. Eng.* **2018**, *2018*, 8093719. [CrossRef]
20. Wang, C.; Gao, H.; Wang, Z.; Chen, G. Model test of abutment on soft soil retaining eps composite soil. *J. Nanjing Tech. Univ. Nat. Sci. Ed.* **2017**, *39*, 118–123.
21. Xie, D. *Soil Dynamics*; Xi'an Jiaotong University Press: Xi'an, China, 2018.
22. Das, B.M.; Luo, Z. *Principles of Soil Dynamics*, 3rd ed.; Cengage Learning: Boston, MA, USA, 2017.
23. Gao, H.; Bu, C.; Wang, Z.; Shen, Y.; Chen, G. Dynamic Characteristics of Expanded Polystyrene Composite Soil under Traffic Loadings Considering Initial Consolidation State. *Soil Dyn. Earthq. Eng.* **2017**, *102*, 86–98. [CrossRef]
24. Rocco, N.; Luna, R. Mixtures of clay/EPS particulates and undrained shear strength. In *Geo-Congress 2013: Stability and Performance of Slopes and Embankments III*; American Society of Civil Engineers: Reston, VA, USA, 2013; pp. 2059–2068.
25. Bao, X.; Jin, Z.; Cui, H.; Chen, X.; Xie, X. Soil liquefaction mitigation in geotechnical engineering: An overview of recently developed methods. *Soil Dyn. Earthq. Eng.* **2019**, *120*, 273–291. [CrossRef]
26. Silveira, M.; Calheiros, A.; Casagrande, M. Applicability of the Expanded Polystyrene as a Soil Improvement Tool. *J. Mater. Civ. Eng.* **2018**, *30*, 06018006. [CrossRef]